Mitigating Humping Using NIR Dual Beam for Welding 1.4404 Stainless-Steel Sheets

Elie Haddad*1,2, Muratcan Dogan³, André Häusler¹, and Alexander Olowinsky¹

¹Fraunhofer Institute for Laser Technology ILT, Aachen, Germany
²RWTH Aachen University, Chair for Laser Technology LLT, Aachen, Germany
³FH Dortmund, University of Applied Sciences and Arts, Dortmund, Germany
*Corresponding author's e-mail: elie.haddad@ilt.fraunhofer.de

The occurrence of the humping phenomenon limits the achievable welding speed in laser beam micro welding processes, thereby constraining reductions in processing time when joining 1.4404 stainless-steel sheets. This weld defect manifests as periodic protuberances along the weld seam surface and negatively affects the mechanical integrity and leak-tightness of the joint. The humping threshold – the welding speed at which these irregularities appear – is typically reached starting around 30 m/min, depending on laser beam characteristics and material properties. The formation of humps is influenced by multiple factors, with melt pool dynamics and flow velocity identified as key contributors. These can be affected by the intensity distribution of laser power. In this work, the effect of introducing an additional laser beam in two configurations to achieve different intensity profiles is investigated. The analysis focuses on hump height and frequency, the presence of pre-humping and humping effects, and weld seam width. The results indicate that dual beam configurations can reduce or eliminate humping under certain conditions, suggesting a stabilization of the keyhole and melt pool dynamics. The findings contribute to a better understanding of humping suppression mechanisms and support the potential for increasing welding speeds beyond 30 m/min without compromising weld seam quality.

DOI: 10.2961/jlmn.2025.03.2014

Keywords: laser beam micro welding, humping phenomenon, dual beam welding, welding speed, melt pool dynamics, stainless-steel, intensity distribution.

1. Introduction

Humping is a well-documented welding defect characterized by the formation of seemingly periodic, bead-like protrusions along the weld bead surface. These irregularities not only deteriorate the mechanical strength of the weld seam but also compromise its leak-tightness, making the mitigation of humping critical for achieving high-integrity joints in applications requiring stringent reliability, such as those involving thin sheets of 1.4404 stainless steel. A typical manufacturing application is the production of metallic bipolar plates for proton exchange membrane (PEM) fuel cells. Bipolar plates (BPP) serve to distribute reactant gases, collect current, and manage water and heat within the fuel cell stack. Since each fuel cell stack requires hundreds of plates, the mass production of bipolar plates demands high welding speeds to ensure cost-effective manufacturing. [1] Given that the typical thickness of bipolar plates ranges from 0.05 mm to 0.2 mm, precision and weld quality are paramount, and defects like humping are particularly detrimental because they can cause leakage or electrical resistance issues. Thus, developing welding techniques that enable stable, high-speed joining without introducing surface irregularities is vital for advancing the scalability and reliability of fuel cell technology. [2]

Numerous models have been proposed to explain the occurrence of humping, focusing on fluid dynamics, surface tension effects, and melt flow instabilities. For arc and electron beam welding, explanations include Rayleigh [3] and Kelvin-Helmholtz instabilities [4], melt flow induced by arc pressure [5], and wall jet effects from filler droplet impact [6]. In laser welding, the phenomenon is often linked to rapid melt flow, evaporation-induced recoil pressure, and unstable keyhole geometries [7]. While prior research identifies the end of the melt pool as the critical region where humping manifests, a complete mechanistic understanding remains elusive [8]. Recent studies have highlighted the role of keyhole shape and molten pool behavior in initiating and evolving humping. Swelling at the rear of the keyhole – driven by oscillations, local keyhole collapse, and insufficient melt drainage – has been recognized as a precursor to humping. Moreover, the evolution of this swelling, determined by the available cooling time and melt flow characteristics, dictates whether it flattens or solidifies into a hump [9]. To suppress humping, innovative approaches such as dual beam laser systems and beam shaping techniques have been explored. Specifically, superimposed core-ring intensity distributions have shown promise in stabilizing keyhole morphology, widening melt pools, and significantly reducing hump formation [10]. Dual beam arrangements on the other hand offer higher flexibility with the settings and adjustments of the energy distribution, allowing for example the beams to move parallel to each other, concentric or even with one beam trailing the other one. Beyond single-beam approaches, prior research on multi-focus or dual-beam welding has consistently shown that spatially distributed energy input can improve process stability. For instance, multi-focus laser welding using a reflective splitting mirror demonstrated that as the number of focal points increases, multiple beams can form a common keyhole, thereby stabilizing the melt pool, reducing spatter, and suppressing porosity formation [11]. Similar improvements were reported for aluminum alloy AA 7075, where dual-beam configurations increased weld seam width, improved surface texture, and reduced hot cracking compared to single-beam welding, with the effect depending on beam spacing and orientation [12]. In a broader context, dual-beam CO2 laser welding studies showed that weld surface quality can be significantly enhanced for both steels and aluminum: spatter, hardness variations, and centerline cracking susceptibility were reduced in steel welds, while porosity, irregular beads, and spatter were substantially decreased in aluminum welds. High-speed imaging further revealed that dual beams suppressed vapor plume fluctuations, leading to a more stable keyhole and improved overall process robustness. [13]. While these studies were carried out on different materials, scales, and process conditions, they underline the general potential of dual-beam strategies for suppressing weld instabilities. The present work builds on these concepts by investigating whether analogous stabilizing effects can be realized in high-speed micro welding of thin 1.4404 stainless-steel sheets, where the dominant defect mechanism is the formation of humping.

2. Theoretical background

2.1 Fundamentals about humping formation

The formation of humping during high-speed laser welding results from the complex interplay of molten pool fluid flow, recoil pressure, heat transfer, Marangoni convection, and solidification dynamics. As the welding speed increases, these effects intensify and often interact in destabilizing ways. In high-speed welding, the molten metal is generally treated as an incompressible fluid, and mass conservation within the melt pool is governed by the continuity equation [3]:

$$\nabla \cdot \vec{v} = 0, \quad (1)$$

where \vec{v} represents the velocity field in the molten region. With rising welding speeds, the forward motion of the heat source outpaces the backward replenishment of molten material, leading to a lack of continuity at the rear of the melt pool and causing localized accumulations that solidify into humps [14].

The transport of momentum within the melt pool can be described by the Navier-Stokes equation. At higher speeds, inertial forces outweigh viscous damping, promoting backward melt flow. This flow periodically detaches at the tail of the melt pool, resulting in the formation of discrete humps – an effect confirmed in both simulations and experimental observations [15,16]. A dominant driver of this instability is recoil pressure, which increases with surface temperature at the front of the keyhole. As shown in recent studies [17], elevated recoil pressure pushes molten material rearward, elongating the melt pool and narrowing its trailing edge. When the recoil-induced momentum exceeds the restraining forces of surface tension and viscosity, the melt pool cannot maintain a continuous flow, and flow separation occurs. This results in the periodic deposition of humps along the weld

seam. Thermocapillary convection, or Marangoni flow, further influences melt pool dynamics. Driven by temperature-dependent surface tension gradients, this flow can induce vortex-like motion, especially when steep thermal gradients exist. Such internal circulations may contribute to uneven solidification and promote instability under unfavorable conditions [18,19].

In addition to these thermofluidic mechanisms, Ray-leigh-type instabilities also offer a theoretical basis for humping. In this framework, the backward-flowing molten metal is likened to a cylindrical fluid jet. When the jet length exceeds a critical threshold – typically its circumference – surface tension alone cannot stabilize it. Small perturbations along the jet surface result in variations in local pressure, amplifying into periodic bulges that eventually solidify as humps [18].

Recent comprehensive reviews [7] emphasize that the onset and severity of humping are influenced not only by speed and pressure dynamics but also by the geometric properties of the weld and the spatial distribution of laser intensity. Specifically, a smaller melt pool cross-section at high speeds is more prone to instability, especially when high energy density is concentrated at a single point.

2.2 Mitigation strategies

In recent studies, several strategies are pursued to suppress humping. [20] revealed that the onset of humping is strongly linked to rear melt pool instability driven by recoil pressure at high speeds. By combining X-ray imaging with numerical simulation, they introduced a dimensionless humping index that successfully predicts the transition from stable to unstable welding. Their results also demonstrated that hump formation is cyclical. Each time the molten pool length decreases below a critical value, it can no longer store the backward-directed melt, leading to periodic accumulation and solidification into humps. The solidification line at the rear of the molten pool is also decisive: insufficient melt replenishment there has been shown to accelerate hump initiation [20].

In parallel, [8] demonstrated that using ring-shaped beam profiles effectively suppresses humping by altering the intensity distribution around the keyhole. Their experiments showed that ring-mode beams reduce localized recoil pressure, promote smoother melt pool flow, and enhance overall stability compared to conventional Gaussian profiles. These effects are particularly beneficial in high-speed welding of thin sections, where conventional beams tend to induce instability [8].

In [21] the role of melt pool geometry in influencing humping behavior is highlighted. Their experiments showed that smaller or highly elongated melt pools tend to be less stable, increasing the risk of hump formation. Conversely, a wider and deeper melt pool cross-section – achieved through a static ring-shaped beam – can significantly improve weld stability, particularly regarding cracks and humping. These findings underscore the importance of controlling weld aspect ratio and thermal distribution to mitigate humping.

3. Methodology

3.1 Experimental setup

To carry out the tests in the context of this paper, the design of the system for laser beam welding is shown in Fig.

1. The laser fiber of laser #1 (1) is inserted into the collimating unit (2) of the deflection unit #1 (3). Analogously, the laser fiber of laser #2 is also connected to the collimating unit of the deflection unit #2 (4). Both deflection units are used in combination with a rayspector module (5) and are mounted using a manual z-axis (6) for smaller range adjustments of the z-position.

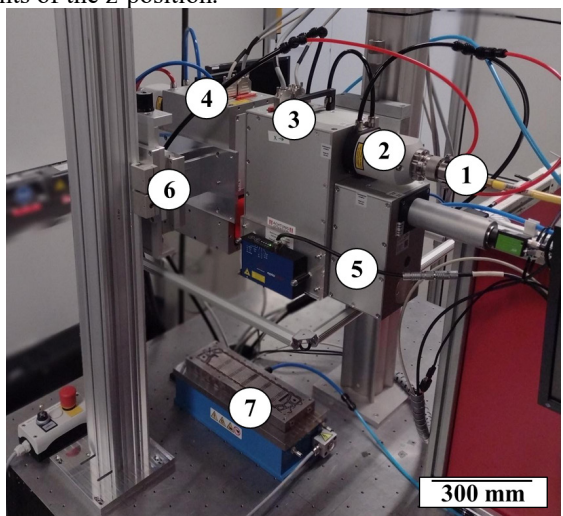


Fig. 1 Experimental setup with laser fiber (1), deflection units (3 and 4), rayspector module (5), manual z-axis (6) and clamping fixture (7).

The samples are processed on an electromagnet base with a clamping fixture to ensure that a technical zero gap is reached (7). The sheets are made of 1.4404 (also known as AISI 316L or X2CrNiMo17-12-2) stainless steel, thickness 0.1 mm each, with chemical composition and mechanical properties typical for PEM fuel cell bipolar plates. Since 1.4404 stainless steel itself is non-magnetic, a clamping mask is placed on top of the sheets and an additional plate with a groove in the middle is placed under the sheets on the magnet. The mask and the underlying plate are both made of a ferritic steel. The beam sources used for the experiments are two SPI red Power Qube single mode fiber lasers from SPI, Southampton (UK) with a maximum output power of P = 1000 W and a wavelength of 1064 nm. For the beam deflection, two Axial Scan Fiber 30 (AS-F 30) units from Raylase GmbH, Weßling, Germany, are employed to accomplish the welding path.

There are several methods to mount multiple raylase processing heads (up to four heads). Typical combinations for a dual beam concept are the face-to-face or the side-to-side formations. For the work in this paper, the chosen method is the face-to-face formation, which is shown in **Fig. 2**.

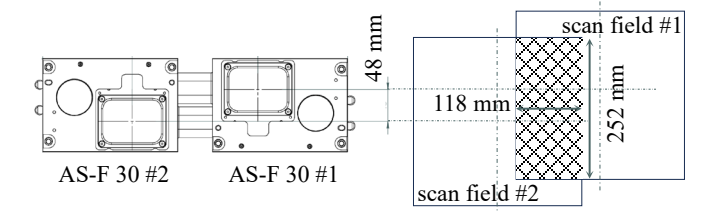


Fig. 2 The face-to-face formation of two AS-F 30 (*left*) and their common processing field seen from above (*right*).

Each individual scan head allows a processing field of 300 x 300 mm². The face-to-face formation allows the expansion of these individual fields to 482 mm in the x-dimension and to 342 mm in the y-dimension, with an overlap area of 252 x 118 mm². Only in the overlap area can both beams be used at the same time and at the same spatial position. Further details regarding the deflection units and lasers are listed in Table 1. With the AS-F #2, the beam diameter in focus is slightly larger than the other one. Both systems are calibrated to realize a working distance of 318 mm and on the same working plane using the multipoint calibration included in the raylase software. The laser caustic and the laser power are measured using respectively a micro spot monitor and a Cube from the company Primes GmbH, Pfungstadt, Germany. Results are provided in the Appendix in **Table 2** and Table 3.

Table 1 Welding system details.

Parameter	-	Unit	-
Wavelength	λ	nm	1064
Max. laser power	each	W	1000
Working distance	W_{D}	mm	318
Focused beam Ø (#1)	d_{F1}	mm	0.042
Focused beam Ø (#2)	d_{F2}	mm	0.046

The beam path through one axial-scan fiber 30 is illustrated schematically in **Fig. 3**. The laser beam – shown in red – is first collimated and then reflected using a 45° reflective mirror onto a moving lens, which determines the working distance. After that, the beam passes through the focusing lens and is reflected once more using a dichroic mirror onto the galvanometric controlled mirrors, which are responsible for realizing the welding contour. The beam shown in blue in the rayspector module represents the light that reaches a camera after being transmitted through the dichroic mirror and reflected onto the camera chip. The main welding parameters include laser power (P_1 and P_2), welding speed (v_1 and v_2), the position of the beam spots relative to each other (Δ) and the defocusing distance – proportional to the size of the second beam spot d_{F2} .

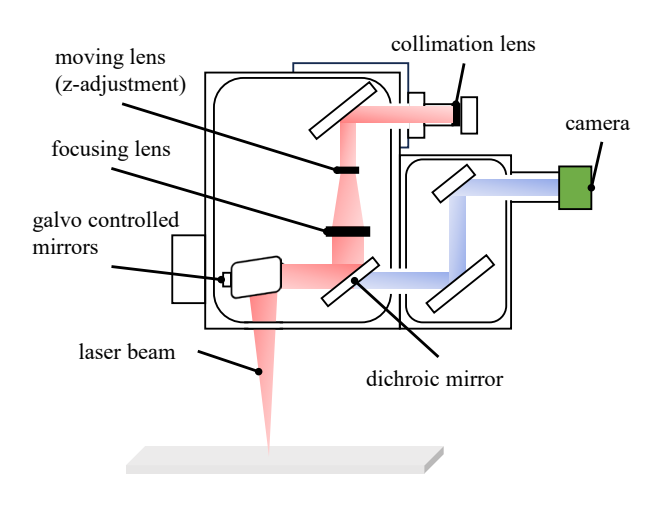


Fig. 3 Beam path through one of the deflection units.

3.2 Design of experiments

The humping phenomenon, which is induced at high flow speeds in the weld pool due to the flow around the keyhole, is to be investigated in more detail when using dual beam welding. In [22], it is shown that when the entire seam cross-section is melted by dual beam welding, the vapor capillary expands both longitudinally and transversely to the welding direction. This reduces the flow speed in the weld pool, so that less ejection can be expected at the end of it, due to the lower kinetic energy. Therefore, it can be assumed that it is possible to influence the humping threshold via a dual beam solution. Improvements in seam quality are to be expected due to the stabilization of the process. Based on this, tests are carried out to determine the suitability of the described approaches for welding thin stainless-steel sheets. The results from the dual beam welds are examined in comparison to the single beam welds. The number of humps per weld (humping frequency) and the average hump height are considered as the evaluation criteria. The weld seam width and in some cases the weld seam root are also measured and evaluated. For this purpose, two different test series are carried out:

- lap welding with a side-by-side arrangement of the laser beams
- lap welding with concentric laser beams, with one beam out of focus

In the following, the experimental procedure is described in detail.

Side-by-side beams arrangement

By arranging the two laser beams transverse to the welding direction, the geometry of the vapor capillary and the flow behavior in the weld pool are to be influenced, while additionally varying the distance between the two laser beam spots. The laser beams are focused on the sample surface, so the welding takes place at focal distance. Lap welding with dual beam and arranging the two laser beams transversely is shown schematically in **Fig. 4**.

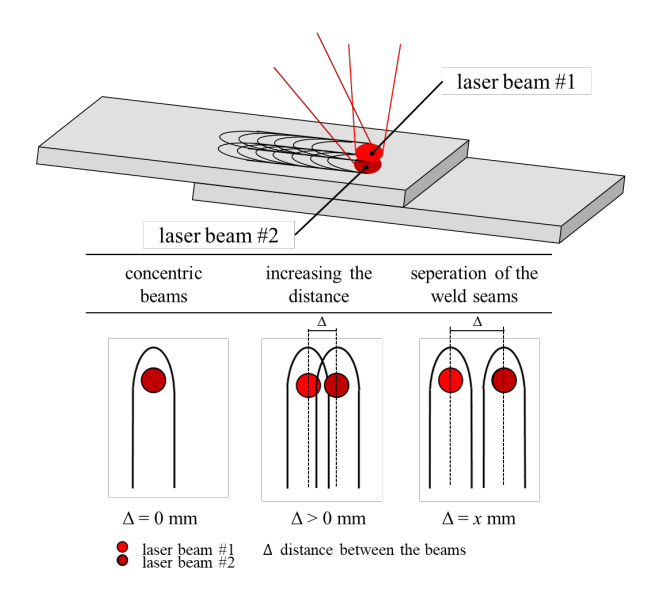


Fig. 4 Schematic explanation of the side-by-side beam arrangement with varying distance between the laser beam spots.

At the beginning, the process has a direct overlap of the two laser beams ($\Delta=0$ mm, concentric spots), so that a single depth capillary can be assumed. In the further course, the distance between the two laser beam spots is increased ($\Delta>0$ mm), whereby a broader surface of the welding can be assumed. After a certain distance, the vapor capillaries are fully separated, and the distance is large enough to cause two individual weld seams to be formed ($\Delta=x$ mm). However, the value for x is unknown and must be experimentally deduced. The test plan for the execution of the side-by-side arrangement is presented in the Appendix in **Table 3**.

Concentric arrangement with enlargement of one beam spot

Using this method, an out of focus laser beam with lower laser power is directed onto the workpiece surface while simultaneously using the other focused laser beam with the usual intensity needed to weld. It resembles the previous arrangement with $\Delta = 0$ mm, in this one however, the z-position of one of the beams is varied to have it in an out of focus state on the workpiece surface (z shift). The aim is to produce a deep, continuous weld seam using the focused laser beam. The defocused laser beam is intended to realize preand post-heating effects, thus causing a smoothing of the seam surface, similar to effects observed while using ring mode lasers. The additional intensity increases the melt pool temperature, which in turn modifies the surface tension and affects melt flow behavior. The enlargement of the weld pool area around the vapor capillary is expected to reduce the high melt flowing speed. This mechanism is consistent with earlier findings: ring-shaped beams widened the melt pool and promoted smoother weld seam surfaces [8]. Fig. 5 illustrates the lap welding process with the concentric arrangement of the beams, while one of the beams is out of focus causing it to have a larger beam diameter d_{F2}.

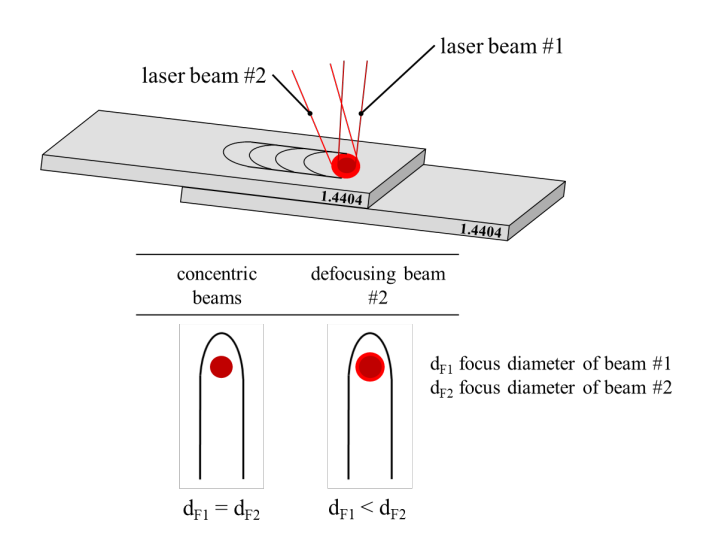


Fig. 5 Schematic explanation of the concentric beam arrangement with the defocusing of laser beam #2.

3.3 Calibrating the beams

To realize the planned beam arrangements for the experiments presented in this paper, the deflection units must first be calibrated to ensure that the laser beam spots are synchronized and spatially aligned. Both lasers are controlled by a single PC equipped with two SP-ICE-3 control cards, which also manage the deflection units. During welding, the sample remains stationary while the laser beams are moved. To ensure synchronized beam availability and motion on the sample surface, the Rayguide software (scanner software by Raylase, Weßling, Germany) offers the possibility of sending the job to the control cards, which is the option used in this work. Starting the welding job is done by using a hardware trigger. The synchronization of the laser beams is examined by using high speed camera recordings using a Photron FASTCAM SA 5 (Tokyo, Japan). Any temporal offset is compensated using the laser jump delay under the pen settings in the rayguide software. For each deflection unit, a separate job is created. The position of the laser beams is adjusted by moving the welding lines in the separate jobs to a fictitious overlap position in both scanning fields. Spatial offsets are then measured using a digital microscope (VHX-6000, Keyence, Osaka, Japan), respectively. The calibration is performed iteratively by readjusting the positions and timing delays until the microscope images show a single, overlapping seam and the high-speed video confirms that both laser beams strike the sample simultaneously.

4. Results and discussion

As described in section 2, several factors lead to the occurrence of the humping phenomenon. The welding speed is one of the defining factors. Simultaneously, the severity and type of humping as well as the periodicity vary depending on the used laser power and the welding speed. In a first step, some welding trials are carried out to outline the process window. During these trials, the laser power is varied in steps of 50 W between 100 W and 1000 W, while simultaneously varying the welding speed in 50 mm/s steps between 500 mm/s and 1000 mm/s. The results from these trials are presented in **Fig. 6**.

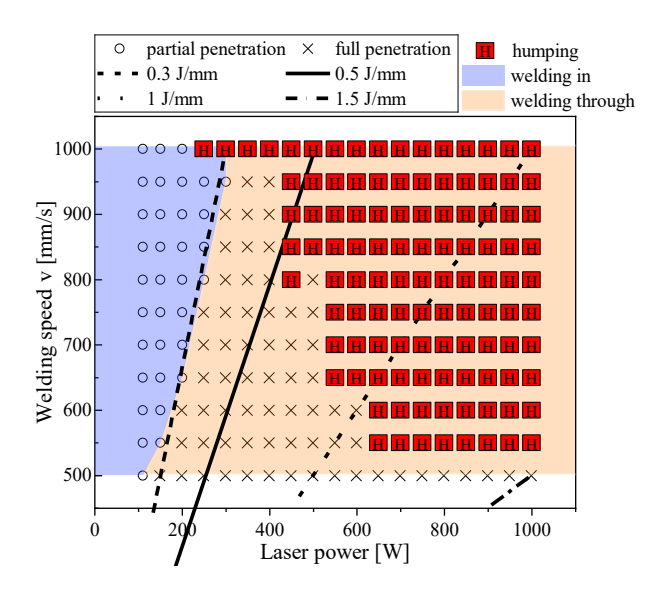


Fig. 6 Process map of single-beam welding trials with varied welding power and speed.

Below the line energy of 0.3 J/mm, full penetration does not occur. Notably, the welding tests using a speed of 1000 mm/s show that humping can take place at lower power levels (<300 W), with the welding speed being the driving factor for the occurrence of the defect. Further increasing the power also negatively impacts the occurrence of humping: with the laser power of 650 W, humping takes place at the relatively low welding speed of 550 mm/s. The trials, where humping occurs, are marked accordingly. Using a welding speed of 500 mm/s leads to hump-free weld seams with the used setup (in this study, a weld seam was defined as hump-free if no protrusions exceeding 20 µm in height (relative to the seam surface) were detected along the weld length, based on 3D surface measurements). The parameter combination P = 400 W and v = 950 mm/s also shows no humping at an increased welding speed, which further highlights the role of the welding power. Based on previous research, laser welding with full penetration minimizes distortion and shape error [23], so for the following trials with the dual beam setup, the parameter combination P = 400 W and v = 1000 mm/s is chosen as a reference.

The welding result is shown in **Fig. 7**. As mentioned before, the number of humps and the humping height are used as evaluation criteria. These should help form a deeper understanding to the variations within the occurrence of the humping phenomenon itself. Using 3D panorama images facilitates identifying humping points and their total number in a weld seam as well as determining their height. Additionally, the weld seam width and the root width are also used to further evaluate the results. The average humping height reached with the parameter settings from the single beam welding is 0.068 mm and the average number of humps is 18.

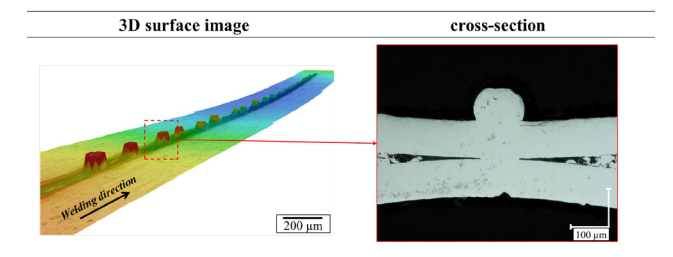


Fig. 7 3D surface image and cross-section image of a humping ridden sample welded with single beam, P = 400 W, v = 1000 mm/s.

Side by side arrangement

Fig. 8 shows the evaluation of the welding results regarding the number of humps per weld seam as a function of the distance between the two beam spots in the side-by-side arrangement. Each parameter set is repeated five times (n=5) to test reproducibility and to assess fluctuations between the single trials. With an increasing distance between the beam spots, the overlap is reduced: at zero, the beams are concentric, at 0.02 mm, the overlap is 50 %, at 0.04 mm, the beams are almost tangential and at 0.05 mm the beam spots are no longer overlapping, but the individual molten pools do not start to separate until a distance of 0.15 mm.

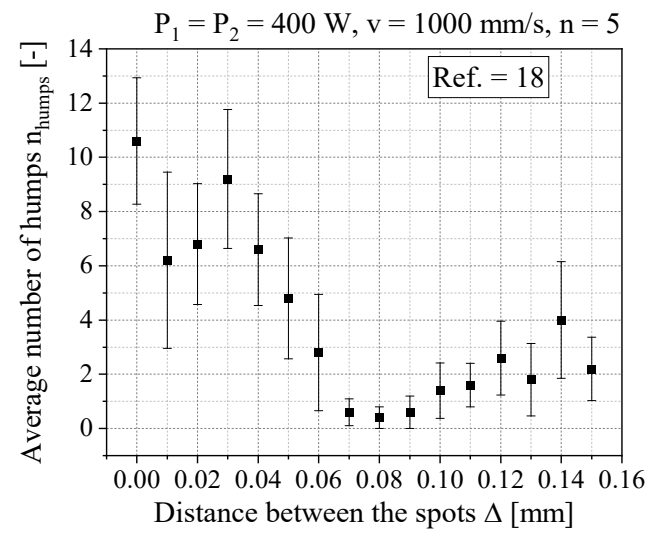


Fig. 8 Humping frequency depending on the distance between the laser beam spots in dual beam side by side configuration with $P_1 = P_2 = 400 \text{ W}$ and v = 1000 mm/s. The reference value (Ref. = 18) corresponds to the average from single-beam welding.

In this evaluation, the distance between the laser beam spots Δ varies from 0 to 0.160 mm. The laser power for each beam is set to 400 W, and all tests are conducted without beam oscillation. For comparison, the average from weld seams produced via single beam welding is used as a reference. The laser beams are focused on the workpiece surface, so the welding takes places at focal distance with $d_{\rm F1}=0.042$ mm and $d_{\rm F2}=0.046$ mm. The results show that humping is generally suppressed in dual beam welding compared to single beam welding, with the highest number of humps recorded (13) being well below the reference from

the single beam welding (18). Particularly starting from a distance of 0.07 mm, the number of humps fluctuates but is kept below an average of approximately six humps per weld. The lowest average number of humps (0.4) is reached with 0.08 mm, where two out of five samples exhibit one hump each. The curve of the number of humps per weld shows a somewhat sinusoidal with a reduction in amplitude trend. One possible explanation for this behavior is that at distances lower than < 0.07 mm, the overlap between the molten pools is too large to have a positive effect on the flow speed of the molten material. The local minimum at $\Delta = 0.08$ mm may be attributed to an optimal overlap between the two melt pools: at this distance, flow velocity is sufficiently reduced to prevent hump accumulation, but the pools are not yet fully separated. At larger distances, the stabilizing effect diminishes, and the frequency of humping rises again. The additional energy input from the effects of the two parallel moving beams partially suppresses humping formation. The dual-beam arrangement modifies the melt pool geometry and redistributes recoil pressure over a broader area. This enlargement of the molten pool lowers peak flow velocities at the rear of the pool, thereby reducing the tendency for periodic flow separation. Similar findings have been reported by Xie et al. [24], who showed that dualbeam welding enlarges the weld pool, stabilizes the keyhole, and decreases the oscillation amplitude of fluid flow, thereby mitigating defect formation. As a result, hump formation is partially suppressed compared to single-beam welding. The results also show a larger fluctuation illustrated with the standard deviations, which appear to generally decrease starting 0.07 mm. At a beam distance ≥ 0.15 mm, the results show that the weld seams have first signs of separation along the weld line on the surface. At 0.016 mm the separation between the individual welding lines is increased and the results can no longer be included in the evaluation. Examining the lower side of the welded samples shows that the separation at the root of the weld seam shows its first sign at 0.1 mm distance and the roots are fully separated at 0.12 mm.

A possible explanation for the positive results is the increase caused by the second beam to the size of the molten pool. An increased area of melt around the keyhole triggers a decrease in the flow speed in accordance with the continuity equation. According to the continuity equation, an enlargement of the molten pool cross-sectional area around the keyhole is expected to reduce the average flow velocity. While full metallographic cross-sections are not in the scope of this paper, the measured seam widths, and root widths (Appendix, Table 4 and Table 6) clearly indicate that the dual-beam configuration produces a significantly larger molten area compared to single-beam welding. The broader weld pool implies reduced average flow velocity, which provides a plausible explanation for the observed partial suppression of humping. Further factors such as effects on the surface tension, liquidity of the melt, and slowing down the cooling of the material due to the second beam can also contribute to the suppression of humping. However, humping is not eliminated, meaning that the threshold for the onset of the welding defect is still reached in most samples.

Fig. 9 shows the evaluation of the welding results regarding the average humping height as a function of the distance between the two beam spots in the side-by-side arrangement.

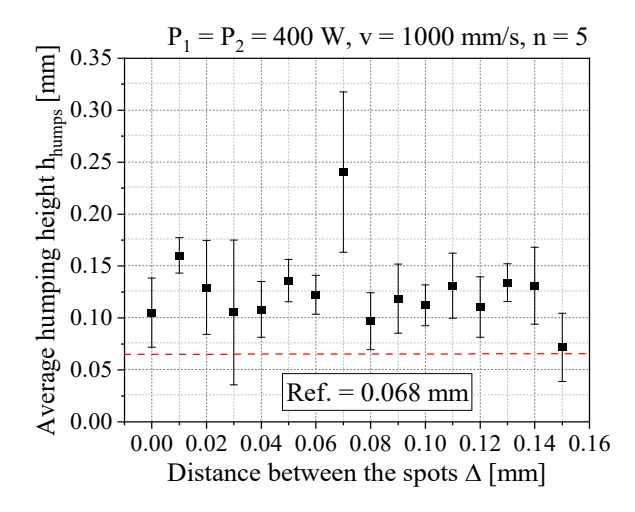


Fig. 9 Variation of the humping height depending on the distance between the laser beam spots in dual beam side by side configuration with $P_1 = P_2 = 400$ W and v = 1000 mm/s. The dashed line (Ref. = 18) represents the average humping frequency observed in single-beam welding trials, used here as a reference baseline.

Here, the weld seams that exhibit no humping are excluded from the evaluation. The average humping height is calculated by measuring the height of each hump in a humping ridden sample and averaging the heights over the total number of humps, and then by calculating the average height from all five trials (only when humping occurs).

Analysis of the humping height indicates a small fluctuation between the adjusted distances. For dual beam welding, the humping height is often twice as large as those observed in single beam welding, with an average of approximately 0.126 mm compared to 0.068 mm for single beam welding. In most of the welded samples, the largest humping point occurs shortly after the start of the weld seam. A plausible explanation for this difference in the humping height is the increased molten pool size in dual beam welding, which can either be attributed to the higher intensity when the beams are concentric or a combination of the two molten pools following the keyholes of the singular beams. A higher molten pool size leads to a higher amount of melt that can get accumulated during the backward flowing, when the critical flow speed for humping is achieved. At the distance of 0.07 mm the largest fluctuation occurs, also it shows an outlier in comparison to the other data points. The reason for this is that humping occurs in three out of five samples with only one hump per weld seam, leading to an increased height, since this hump occurs at the start of the weld seam with an increased height, similar to the other humping cases in these trials.

The comparison of the 3D surface images shows that when welding with a single beam, the humps are small and lie close together in large numbers. In contrast, dual beam welding with a side-by-side arrangement of the beams and a distance of 0.04 mm for example shows a small number of humps, but with a larger humping height, which further confirms the explanation with the larger molten pool. Only in the case of 0.15 mm distance between the beam spots, is the humping height similar to the one achieved with single beam welding, indicating here a start in the separation of the

molten pools, which then leads to two individual parallel weld seams.

Fig. 10 shows the influence of the side-by-side arrangement of the two laser beams on the weld seam width and the weld seam root with the example of $\Delta = 0.09$ mm and $\Delta = 0.12$ mm. With 0.12 mm defocusing distance the roots of the weld seams are completely separated and appear as two individual lines.

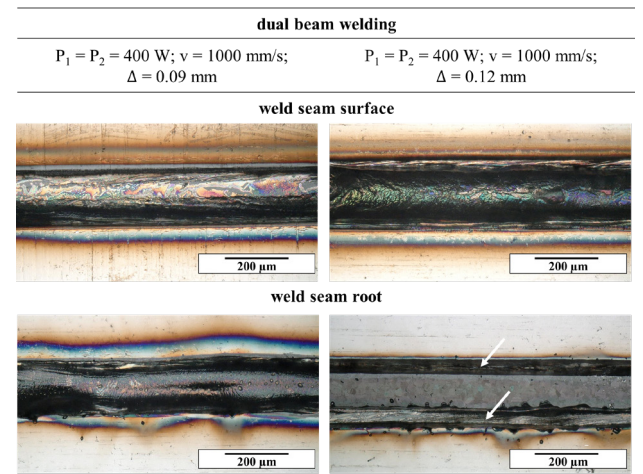


Fig. 10 Seam and root width comparison in dual beam side by side configuration ($\Delta = 0.09 \text{ mm } \& 0.12 \text{ mm}$).

The weld seam width for $\Delta=0.09\,\mathrm{mm}$ reaches 0.191 mm on average, while the weld seam width for $\Delta=0.12\,\mathrm{mm}$ reaches 0.215 mm on average. With single beam welding, the weld seam width reaches about 0.09 mm, while with this dual beam welding strategy, the width is almost doubled and reaches on average for all samples about 0.194 mm, with the largest average width amounting to about 0.241 mm with $\Delta=0.15\,\mathrm{mm}$, which can be expected due to the increased distance between the beam spots.

When evaluating all the trials values between 0.132-0.241 mm are recorded for the weld seam width with dual beam welding. With a further increase in the distance to 0.16 mm, two individual seams are created again, so the distance is too large to realize a unified weld, even on the surface. It is also noticeable that from a distance \geq 0.12 mm, two separate root beads appear on the rear side of the welded sample.

In conclusion, the reduction in humping frequency observed in this dual beam welding strategy can be attributed to a decrease in melt flow velocity and a broader, more stable melt pool. This aligns with predictions from the continuity equation, where increased melt pool cross-sectional area (A) corresponds to reduced flow velocity (v), assuming constant volumetric flow rate (Q). A larger A from dual-beam input therefore lowers v, possibly also diminishing the recoil driven backward flow responsible for hump formation.

Concentric arrangement

Analogously, trials are carried out with the concentric arrangement of the laser beams during the dual beam welding. In this arrangement, as explained in 4.4, one laser beam is focused on the surface of the workpiece while simultaneously the other one is operated at a different distance than the focal distance. This causes the beam diameter, which

meets the workpiece surface, to be enlarged and the intensity to drop, since the laser power is distributed over a larger surface area, thus reducing the local power density. The beam diameter increases as the distance from the focal point increases. Fig. 11 shows the results of the dual beam welding with the concentric arrangement.

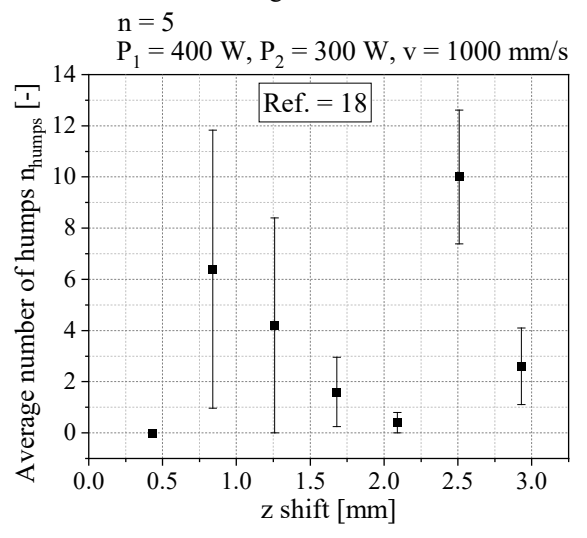


Fig. 11 Humping frequency as a function of the beam defocus distance in concentric dual beam configuration with $P_1 = 400 \text{ W}$, $P_2 = 300 \text{ W}$ and v = 1000 mm/s. The reference value (Ref. = 18) corresponds to the average from single-beam welding.

In this analysis, the distance from the focal point is varied with the aim to find a setting, where humping is suppressed. For this, the adjustment of the z-position for the welded line is carried out in the rayguide software and the focal position is pushed further into the workpiece (downwards), so that the larger diameter meets the sample surface.

In the evaluation under consideration, the distance from the focal point is varied between 0 and 2.93 mm for laser beam #2, while P₂ is set at 300 W. The primary objective of this setup is to apply a moderate, spatially distributed heat input around the focused beam to pre- and post-heat the weld zone, thereby altering melt pool dynamics. The laser power of the focused laser beam (beam #1) is $P_1 = 400$ W. This setting remains similar to the single beam welding tests, with the aim of isolating the extra effects from the second beam. This parameter setting is chosen based on the preliminary tests from the single beam welding, since it is the setting at which full weld penetration is consistently achieved at high welding speeds. With this setting, humping starts at \geq 950 mm/s, so it represents the edge of the onset of the instability and allows enough room for humping suppression at higher speeds with the dual beam setup. The tests are carried out without oscillation. Notably, a significant reduction in humps is achieved compared to single beam welding. On average, the values are 3.6 humps per weld seam, whereas a value of approx. 18 is achieved with single beam welding. The values for dual beam welding in the concentric arrangement are also reduced compared to the side-by-side arrangement (about 3.9 humps). The diagram in Fig. 11 also shows that the largest reductions in humping are achieved with distances 0.429 mm and 2.089 mm from the focal point, corresponding to beam diameters of 0.052 mm and 0.091 mm.

The values for the beam diameter are derived from the caustic measurement, the results of these measurements are shown in the appendix. According to the literature, one possibility to reduce the frequency of humping is by increasing the beam diameter leading to a larger weld pool. Starting from a distance $\geq 0.839 \,\mathrm{mm}$ (focus diameter values \geq 57 µm), however, the frequency of humping increases again so that the number of humps per weld seam increases and reaches values of up to approx. 6 per weld seam. These values are still lower than the values achieved with single beam welding. A comparison of the surface images shows that the humps are small and close together in large numbers during single beam welding. In contrast, dual beam welding with a concentric arrangement, with laser beam #2 1.259 mm out of focus, has a small number of humps (about 4). In this case, the humps tend to have a rather elongated form, are spaced at larger intervals and have comparatively a similar humping height to single beam welding or are slightly larger. The humping height is reduced at the defocus distance of 2.929 mm (0.112 mm beam diameter of laser#2) and reached 0.032 mm, its lowest value. Similar to the case of the side by side arrangement, here too, the largest hump is formed shortly after the start of the weld seam. This can be largely attributed to differences in the coupling behavior of the laser beams.

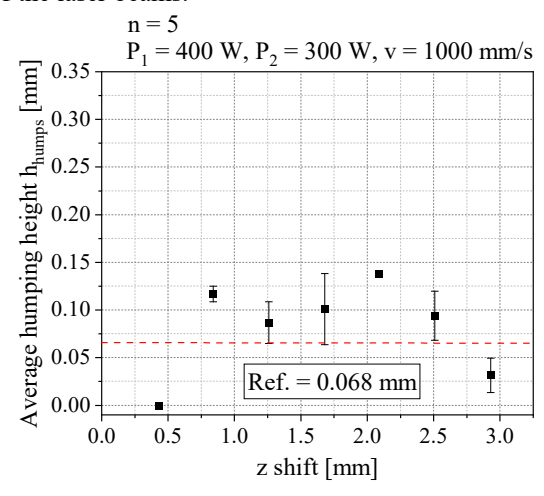


Fig. 12 Variation of the humping height depending on the beam defocus distance in concentric dual beam configuration with $P_1 = 400 \text{ W}$, $P_2 = 300 \text{ W}$ and v = 1000 mm/s. The dashed line (Ref. = 18) represents the average humping frequency observed in single-beam welding trials, used here as a reference baseline.

Additionally, the weld seam widths are evaluated. These show that with dual beam welding in the concentric arrangement the seam widths are at most 0.05 mm wider compared to single beam welding. While single beam welding reaches a value of about 0.09 mm, dual beam welding in this strategy reaches values between approx. 0.107-0.138 mm. It is also noticeable that the largest seam width is reached at a defocusing distance of 2.089 mm (focus diameter = 0.091 mm) but decreases for the defocusing distances before and after. Contrary to what can be expected, the weld seam width does not gradually increase with the enlarged beam diameter #2. A possible explanation for this occurrence can be the

instability and uneven intensity distribution in the laser beam spot, once the Rayleigh length is surpassed.

Overall, all dual beam configurations demonstrated a significant potential to mitigate the humping phenomenon under high-speed welding conditions. While the side-by-side approach improved seam width and moderately reduced hump frequency, the concentric beam setup showed substantial reduction in humping in some cases. These findings support the hypothesis that modifying melt pool dynamics and keyhole stability through tailored intensity distributions can enhance weld quality in stainless-steel micro-welding applications.

5. Conclusion

This paper demonstrates that near-infrared (NIR) dual beam laser welding is a suitable method for suppressing the humping phenomenon during high-speed microwelding of 1.4404 stainless-steel sheets. Two dual beam configurations – side by side and concentric – were systematically evaluated and compared with the state of the art single-beam welding. The main findings can be summed up as follows:

- The side-by-side beam arrangement significantly reduced humping frequency, particularly at an adjusted beam spacing of 0.08 mm, where humping is nearly eliminated in all five samples. Though humping height increased due to the enlarged melt pool, overall weld quality improved. The seam width however nearly doubled.
- The concentric beam setup, with one beam defocused, yielded stronger humping suppression reducing the average number of humps from 18 (single beam) to just 3.6. Select defocus distances (e.g., 2.089 mm) also minimized humping height and enhanced result stability.

Across both methods, the dual beam approach successfully influenced melt pool dynamics by altering intensity distributions, reducing recoil pressure effects, and stabilizing the keyhole, thereby extending the process window for high-speed, defect-free welding up and including 1000 mm/s.

While the current configurations already demonstrate good potential, further enhancements and understanding could be achieved through additional experimental and modeling efforts. Future studies could explore following aspects:

- A trailing beam configuration, where one laser beam follows the other at a defined distance. This setup could provide extended post-treatment effects, potentially enabling even greater control over melt flow and solidification dynamics. Trailing-beam strategies have been shown to suppress humping in welding with larger spot sizes as described, for example, in [25]. Whether the same stabilizing mechanisms apply in micro-welding, where spot sizes are on the order of tens of micrometers and tolerances are much tighter, remains unclear. This gap motivates future investigations of trailing-beam configurations under similar conditions like in this paper.
- Beam oscillation strategies in dual beam mode, which may further disrupt instabilities and smooth out temperature gradients.

- The use of different wavelength combinations (e.g., combining NIR with green or blue lasers) to explore wavelength-dependent absorption effects on melt pool behavior.
- Numerical modeling to simulate fluid flow, temperature distribution, and stress formation under various dual beam configurations, helping optimize designs before experimentation.

These directions could pave the way for even more robust and scalable welding strategies, particularly for applications such as fuel cell manufacturing, where speed, precision, and reliability are critical.

Acknowledgments and Appendixes

This work was funded by the German federal ministry for digital and transport in the H2GO project under the funding reference number 03B11027A and supported by the European Union through the Horizon Europe project NEXTBAT (Grant No. 101103983).

Appendix

Table 2 Beam caustic measurement for laser beam #1.

Plane	Position Z [mm]	Radius [µm]
0	26.5	53.255
1	26.74	50.201
2	26.97	46.628
3	27.21	42.941
4	27.45	38.818
5	27.68	35.354
6	27.92	32.145
7	28.16	28.954
8	28.39	24.933
9	28.63	23.133
10	28.87	21.828
11	29.11	21.34
12	29.34	21.609
13	29.58	22.467
14	29.82	24.053
15	30.05	27.039
16	30.29	31.614
17	30.53	34.263
18	30.76	37.367
19	31	42.816

Caustic measured at Position Z = 29.129 mm, Radius = 21.218 μm

Table 3 Beam caustic measurement for laser beam #2.

Plane	Position Z [mm]	Radius [µm]
0	6	97.252
1	6.42	90.510
2	6.83	82.852
3	7.25	76.842
4	7.67	62.976
5	8.08	57.275
6	8.50	50.997
7	8.92	46.226
8	9.33	39.072
9	9.75	33.386
10	10.17	28.166
11	10.58	24.171
12	11	23.179
13	11.42	26.187
14	11.83	28.410
15	12.25	33.625
16	12.67	38.502
17	13.08	44.932
18	13.50	51.657
19	13.92	57.320
20	14.33	64.510
21	14.75	76.671
22	15.17	83.925
23	15.58	90.187
24	16	98.275

Caustic measured at Position Z = 10.991 mm, Radius = 23.093 μ m

Table 4 Average weld seam widths with standard deviations of the side by side arrangement.

Δ [mm]	Seam width [mm]	Standard deviation [mm]
0	0.132	0.022671
0.01	0.151	0.023426
0.02	0.1622	0.016702
0.03	0.1724	0.016847
0.04	0.1716	0.0088
0.05	0.1738	0.019752
0.06	0.1844	0.010669
0.07	0.1704	0.003979
0.08	0.1808	0.008588
0.09	0.191	0.013084
0.1	0.198	0.003162
0.11	0.2096	0.001854
0.12	0.2154	0.0028
0.13	0.2368	0.01260
0.14	0.2378	0.006554
0.15	0.241	0.006228
0.16	0.2646	0.012877
	·	·

Table 5 Test plan for the side by side arrangement.

P ₁ [W]	P ₂ [W]	v [mm/s]	Δ [mm]
400	400	1000	0
400	400	1000	0.01
400	400	1000	0.02
400	400	1000	0.03
400	400	1000	0.04
400	400	1000	0.05
400	400	1000	0.06
400	400	1000	0.07
400	400	1000	0.08
400	400	1000	0.09
400	400	1000	0.1
400	400	1000	0.11
400	400	1000	0.12
400	400	1000	0.13
400	400	1000	0.14
400	400	1000	0.15
400	400	1000	0.16

 Table 6
 Average weld seam widths with standard deviations of the concentric arrangement.

z-shift	D_{F2}	Seam width	Standard deviation
[mm]	[mm]	[mm]	[mm]
0.429	0.052	0.1162	0.008084
0.839	0.057	0.1236	0.010781
1.259	0.068	0.1078	0.002925
1.679	0.076	0.1072	0.007166
2.089	0.091	0.1388	0.012808
2.509	0.105	0.1128	0.011720
2.929	0.112	0.1176	0.0052
2.509	0.105	0.1128	0.011720
2.929	0.112	0.1176	0.0052

Data Availability Statement

The data that supports the findings in this study are available upon reasonable request. Selected data are available after authorization in Coscine with the persistent identifier (PID) http://hdl.handle.net/21.11102/6344f208-a96d-4e06-a6db-6afff084c115 (accessed on June 03, 2025). For further information, please contact the corresponding author.

References

- [1] Y. Wang, L. Zhang, H. Li, and J. Liu: Trans. Nonferrous Met. Soc. China, 30, (2020) 2523.
- [2] S. Karimi, N. Fraser, and E. P. L. Roberts: Mater. Renew. Sustain. Energy, 1, (2012) 3.
- [3] U. Gratzke, P.D. Kapadia, and J. Dowden: Phys D: Appl. Phys., 25, (1992) 1640.
- [4] A. Kumar, and T. Debroy: Weld. J., 85, (2006) 292s.
- [5] E. Soderstrom, and P. Mendez: Sci. Technol Weld. Join., 11, (2006) 572.
- [6] Y. Lei, X.P. Zeng, and H.D. Dong: Robot. Comput.-Integr. Manuf., 63, (2020) 101916.
- [7] A. Patschger, M. Seiler, and J. Bliedtner: J. Laser Appl., 30, (2018) 032409.
- [8] K. Schwarzkopf, S. Burger, L. Chechik, C. Forster, M. Döring, C. Spurk, M. Hummel, A. Olowinsky, F. Beckmann, J. Moosmann, and M. Schmidt: J. Laser Appl., 36, (2024) 042027.
- [9] M. Beck, P. Berger, and F. Dausinger: Proc. of SPIE -Int. Soc. Opt. Eng., (2012) 769
- [10] E. Haddad, M.C. Lach, C. Spurk, M. Hummel, A. Häusler, A. Olowinsky, F. Beckmann, and J. Moosmann: J. Laser Micro Nanoeng., 20, (2025) 1.

- [11] P. Berger, H. Hügel, A. Hess, R. Weber, and T. Graf: Phys. Procedia, 12, (2011) 232.
- [12] Y. Li, W. Wu, J. Chen, H. Zhu, and Y. Zhang: Opt. Express, 32, (2024) 23147.
- [13] M. Rethmeier, T. Seefeld, F. Vollertsen, et al.: Proc. 8th Int. WLT-Conf. Lasers Manuf. (LiM 2017), Munich, Germany, (2017) Contribution 190.
- [14] J. Xie: Weld. J., 81, (2002) 223.
- [15] A. Otto, S. Koch, R. Weber, and T. Graf: Phys. Procedia, 83, (2016) 1415.
- [16] I. Eriksson, J. Powell, and A.F.H. Kaplan: Opt. Lasers Eng., 51, (2013) 735.
- [17] C.Tang, K.Q. Le, and C.H. Wong: Int. J. Heat Mass Transf., 149, (2020) 119172.
- [18] B. Xue, B. Chang, S. Wang, R. Hou, P. Wen, and D. Du: Mater., 15, (2022) 2420.
- [19] Y. Kawahito, M. Mizutani, and S. Katayama: Sci. Technol. Weld. Join., 14, (2009) 288.
- [20] Z.H. Lai, S. Xu, S.J. Clark, K. Fezzaa, and J. Li: Nat. Commun., 15, (2024) 9546.
- [21] F. Nahr, D. Bartels, R. Rothfelder, M. Schmidt: J. Manuf. Mater. Process., 7, (2023) 93.
- [22] H. Hügel, and T. Graf: Laser in der Fertigung., 2. Auflage, (2009) 268. (in German)
- [23] P. Yi, X. Du, Y. Kan, L. Peng, and X. Lai: Int. J. Hydrogen Energy, 40, (2015) 4850.
- [24] X. Xie, W. Huang, J. Zhou, and J. Long, J. Laser Appl. 34, (2022) 022007.
- [25] Y. Pei and J. Shan, Eng. Res. Express 2, (2020) 025031.

(Received: June 30, 2025, Accepted: November 3, 2025)